ACS SENSORS

pubs.acs.org/acssensors

Article

Remote Detection of HCN, HF, and Nerve Agent Vapors Based on Self-Referencing, Dye-Impregnated Porous Silicon Photonic Crystals

Yi-Sheng Lu, Sanahan Vijayakumar, Arnaud Chaix, Brian R. Pimentel, Kyle C. Bentz, Sheng Li, Adriano Chan, Charlotte Wahl, James S. Ha, Deborah E. Hunka, Gerry R. Boss, Seth M. Cohen, and Michael J. Sailor*

Cite This: *ACS Sens.* 2021, 6, 418−428

Read Online

ACCESS | Metrics & More | Article Recommendations | Supporting Information

ABSTRACT: A one-dimensional photonic crystal is prepared from porous silicon (pSi) and impregnated with a chemically specific colorimetric indicator dye to provide a self-referenced vapor sensor for the selective detection of hydrogen fluoride (HF), hydrogen cyanide (HCN), and the chemical nerve agent diisopropyl fluorophosphate (DFP). The photonic crystal is prepared with two stop bands: one that coincides with the optical absorbance of the relevant activated indicator dye and the other in a spectrally "clear" region, to provide a reference. The inner pore walls of the pSi sample are then modified with octadecylsilane to provide a hydrophobic interior, and the indicator dye of interest is then loaded into the mesoporous matrix. Remote analyte detection is achieved by measurement of the intensity ratio of the two stop bands in the white light reflectance spectrum, which provides a means to reliably detect colorimetric changes in the indicator dye. Indicator dyes were chosen for their specificity for the relevant agents: rhodamine-imidazole (RDI) for HF and DFP, and monocyanocobinamide (MCbi) for HCN. The ratiometric readout allows detection of HF and HCN at concentrations (14 and 5 ppm, respectively) that are below their respective IDLH (immediately dangerous to life and health) concentrations (30 ppm for HF; 50 ppm for HCN); detection of DFP at a concentration of 114 ppb is also demonstrated. The approach is insensitive to potential interferents such as ammonia, hydrogen chloride, octane, and the 43-component mixture of VOCs known as EPA TO-14A, and to variations in relative humidity (20−80% RH). Detection of HF and HCN spiked into the complex mixture EPA TO-14A is demonstrated. The approach provides a general means to construct robust remote detection systems for chemical agents.

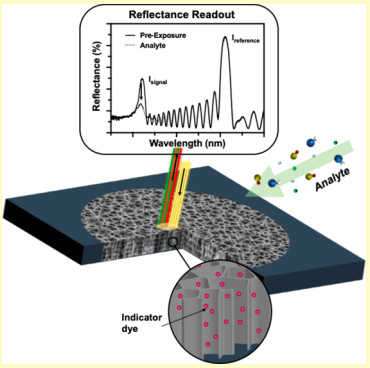

KEYWORDS: *ratiometric sensor, colorimetric sensor, cobinamide, rhodamine-imidazole, optical sensor, toxic industrial chemicals, chemical warfare agents*

There is a longstanding need for simple systems that can remotely detect airborne toxic industrial chemicals (TICs) and chemical warfare agents (CWAs).[1,2] Technologies that meet the criteria of portability, real-time response, and low false positives or false negatives include gas chromatography−mass spectroscopy (GC/MS),[3] ion mobility spectrometry (IMS),[4] and infrared and Raman spectroscopy.[5−8] When low power consumption, small form factor, and low complexity are taken into consideration, point sensor technologies involving surface acoustic wave (SAW),[9] conducting polymers,[10] or metal oxide sensors[11] can provide good sensitivity, but typically provide lower selectivity, compromising false alarm/false positive metrics. Colorimetric indicators, in which the target analyte is detected by a specific molecular interaction with a dye that responds to the event with a change in its electronic structure and thus its color, offer a simple yet powerful means to enhance specificity in point sensors. Many colorimetric indicators have been synthesized that provide high selectivity and sensitivity for the detection of a variety of important environmental analytes: volatile organic compounds (VOCs), explosives, TICs, and CWAs.[12−14] An advantage of colorimetric indicators is that multiple dyes can be incorporated into spatially segregated arrays to allow detection of multiple analytes simultaneously or to increase fidelity by taking advantage of the cross-reactivity of the dyes to different agents.[14−16] Dyes can also show relatively low susceptibility to interference from environmental fluctuations in temperature and humidity—a particular challenge for many point sensors.[17] The increased availability of low-power, high-resolution digital cameras in recent years has been an enabling feature of colorimetric indicators, which has led to increased interest in their use in remote sensing schemes.[18−23] In remote sensing,

Special Issue: Commemorating NJ Tao

Received: September 15, 2020
Accepted: November 13, 2020
Published: December 2, 2020

the sensor element is located a substantial distance from the optical reader, which places limitations on the system related to spatial resolution, extraneous "clutter" in the image field that can obscure the colorimetric signal, and uncontrolled lighting conditions.[23] The problem is compounded by the fact that most organic indicator dyes have broad absorbance bands that are not particularly distinctive compared to the broad range of pigments and dyes commonly present in the environment.

In prior work, we showed that the fidelity of remote detection with an indicator dye can be substantially improved by impregnating the dye in a porous silicon (pSi)-based 1-D photonic crystal.[24] Using a standard pH indicator dye, bromothymol blue, a photonic crystal was prepared with two reflectance (stop) bands: one that overlapped with the absorbance band of the basic form of the dye (the "signal" channel) and the other that appeared in a spectral region where the dye showed minimal absorbance (the "reference" channel). We found that the intensity ratio of the reflectance bands accurately responded to a gas-phase ammonia challenge, and this corrected for large changes in zero-point drift associated with fluctuating probe light intensity. Prepared using an electrochemical anodization process, the pSi system provides a convenient means to fabricate mesoporous 1-D photonic crystals for such applications, allowing the programmatic generation of complex spectral signatures that can be measured from a remote distance by optical reflectance spectroscopy or by hyperspectral imaging.[24−27] The spectral reflectance features from this material are relatively insensitive to fluctuations in temperature over the envisioned operating range of a remote environmental sensor.[28]

While the earlier work demonstrated the remote detection concept for the pSi system, the reliability of the approach for use in "real-world" complex air samples and with changing humidity was not evaluated. Furthermore, it used a simple pH indicator dye, and the question of how generalizable the approach might be to chemical agents other than simple acids and bases was not addressed. Here, we evaluate the selective detection of hydrogen fluoride (HF), diisopropyl fluorophosphonate (DFP), and hydrogen cyanide (HCN) vapors using indicator dyes for which specificity is well established: a rhodamine−imidazole (RDI) complex for detection of HF and DFP, and monocyanocobinamide (MCbi) for detection of HCN. The sensors are tested for their sensitivity and selectivity relative to common environmental interferents and to changes in background relative humidity.

RESULTS AND DISCUSSION

Preparation of pSi Photonic Crystal Sensors. The sensor and detection concepts are outlined in Figure 1. The pSi photonic crystals were prepared by electrochemical anodization of single-crystal Si wafers in an aqueous ethanolic hydrofluoric acid solution using a composite current density−time waveform as previously described,[29] and then chemically modified to improve their performance in ambient environments. For preparation of the photonic crystals, the etching waveform was composed of a sum of two sine waves, such that the photonic crystal that resulted from the process would display two stop bands in the reflection spectrum that could act as "reference" and "sample" channels due to their differing wavelengths (Figure 1). The time-dependent current density waveforms, $J(t)$, used in this work were created following the relationship:

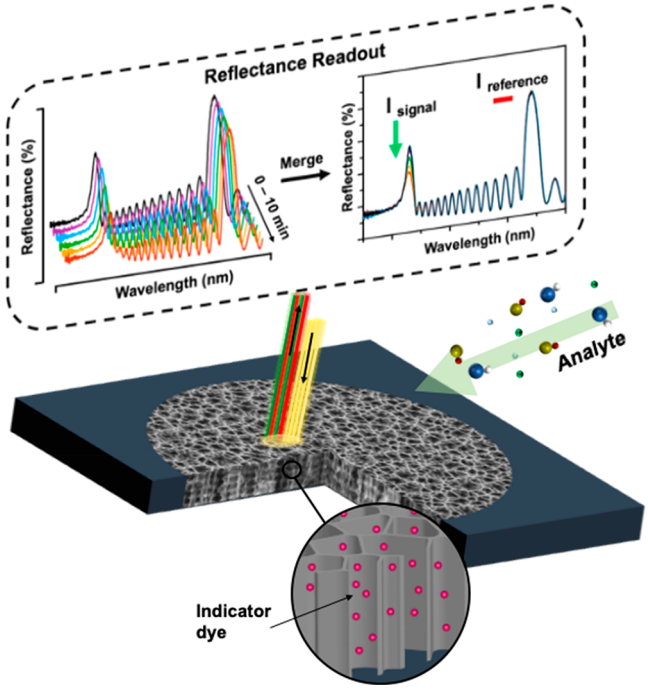

Figure 1. Sensor and sensing approach used in this work. A mesoporous Si photonic crystal is prepared with two stop bands: one that coincides with the optical absorbance of the relevant activated indicator dye (signal channel) and the other in a region of the spectrum where neither activated nor inactivated forms of the dye absorbs (reference channel). The inner pore walls are modified with octadecylsilane to provide a hydrophobic interior, and the indicator dye of interest is loaded into the mesoporous matrix. Analyte binding to the dye is quantified as $I_{signal}/I_{reference}$, where I_{signal} and $I_{reference}$ are the intensities of light reflected at the signal and reference wavelength bands, respectively.

$$J(t) = \left[\frac{J_{max} + J_{min}}{4}\right]\left[\sin\left(\frac{t}{T_1}\right) + \sin\left(\frac{t}{T_2}\right)\right] + \left[\frac{J_{max} + J_{min}}{2}\right] \quad (1)$$

where J_{max} and J_{min} represent the maximum and minimum current density values applied during the etch, and T_1 and T_2 are the periods of the two sine waves used, each of which determined the wavelength of one of the two stop bands in the resulting photonic crystal. These values were determined empirically based on the wavelength of the absorbance maximum for the particular indicator dye of interest. For the HF and DFP sensors (which use the RDI indicator dye), samples with stop bands centered at 520 and 730 ± 10 nm were designed, and for the HCN sensor (which uses the MCbi indicator dye), stop bands centered at 605 and 730 ± 10 nm were prepared (Figure 2). For both sample types, the wavelength of 720−740 nm was chosen for the "reference" band because both of the indicator dyes showed minimal absorbance in this region, either before or after exposure to their intended analytes (Figure 2). The other stop band in each sample was the "signal" band, whose wavelength was chosen to optimally overlap with the absorbance of the colorimetric indicator dye when it interacted with the analyte of interest (Figure S1, Supporting Information).

Surface Modification and Loading of Indicator Dyes. After anodization and prior to loading the indicator dye of interest into the mesoporous matrix, the inner pore walls of the

https://dx.doi.org/10.1021/acssensors.0c01931
ACS Sens. 2021, 6, 418−428

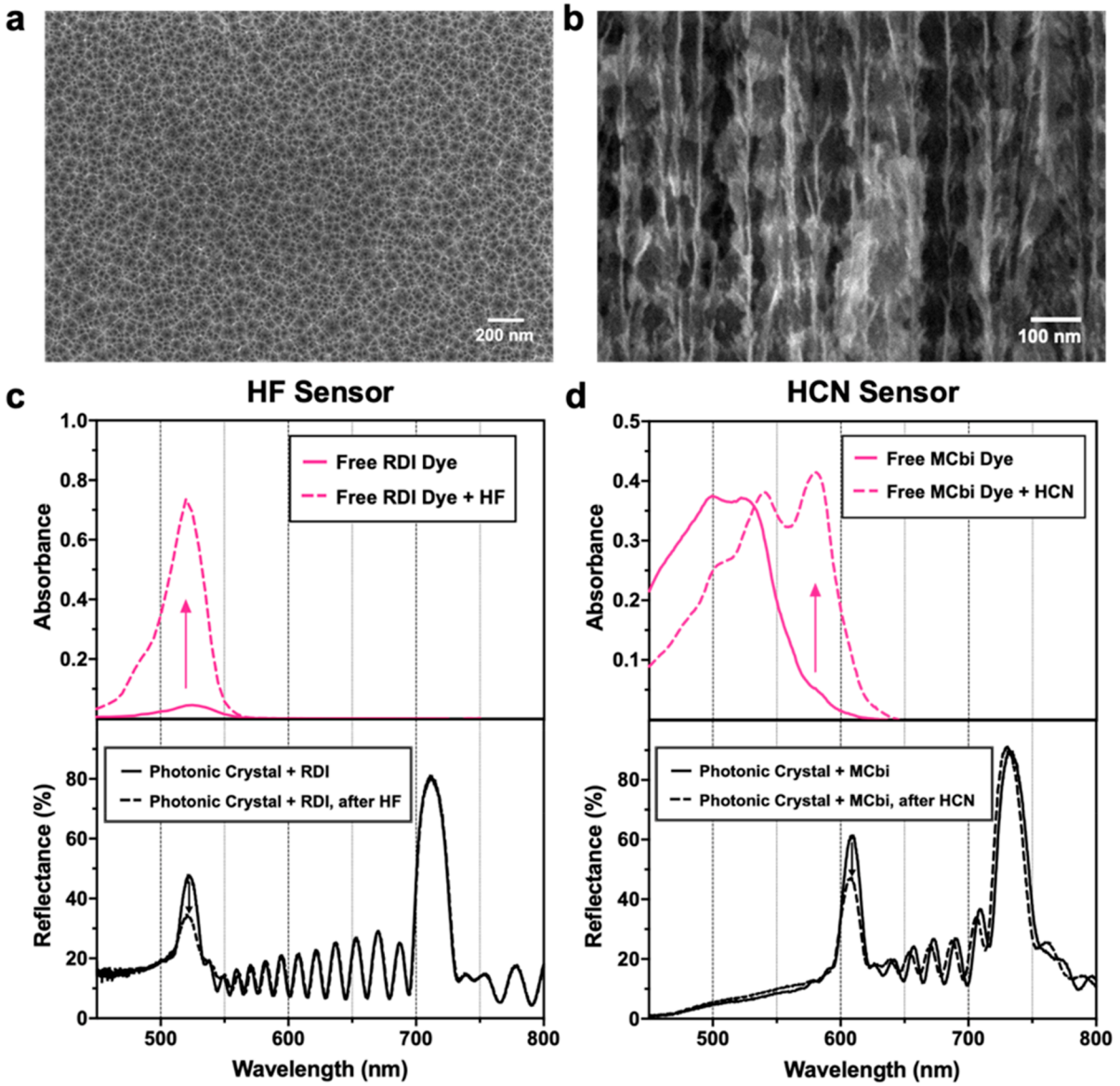

Figure 2. Morphology of pSi photonic crystal sensors and their optical response to analyte vapor challenges. Representative plan-view (a) and cross-sectional (b) scanning electron microscope (SEM) images of the octadecylsilane-modified porous Si photonic crystal, pSi-Si(C_{18}). (c) Representative visible absorbance spectrum of RDI dye in solution (top) and optical reflectance spectrum of RDI dye-impregnated pSi-Si(C_{18}) photonic crystal (bottom), before and after exposure to HF analyte. Absorbance spectrum measured in a 1 cm path length cuvette using RDI dye (2 mM) dissolved in 1:1 (v:v) acetonitrile:dichloromethane. Addition of HF performed by introduction of aqueous HF (48% by mass) sufficient to achieve final [HF] = 17 mM. Optical reflectance spectrum of RDI-impregnated pSi-Si(C_{18}) photonic crystal was measured before and after exposure to HF vapor as described in the text, resulting in the indicated decrease in intensity of the band at 520 nm. (d) Representative visible absorbance spectrum of monocyanocobinamide, MCbi, in solution (top) and optical reflectance spectrum of MCbi dye-impregnated pSi-Si(C_{18}) photonic crystal (bottom), before and after exposure to hydrogen cyanide analyte (diluted in dry dinitrogen). Absorbance spectrum measured in a microplate reader normalized to a 1 cm path length cuvette equivalent using MCbi dye (500 μM) dissolved in ethanol. Addition of cyanide performed by introduction of concentrated aqueous KCN sufficient to achieve final [CN^-] = 500 μM. Optical reflectance spectrum of MCbi-impregnated pSi-Si(C_{18}) photonic crystal measured before and after exposure to HCN vapor as described in the text, resulting in the indicated decrease in intensity of the band at 605 nm.

pSi samples were modified with octadecylsilane to provide a hydrophobic interior, referred to in this work as pSi-Si(C_{18}). The main motivation for this chemistry was to suppress the response of the materials to humidity. In particular, the wavelength maximum of the stop band in pSi photonic crystals is known to shift in response to capillary condensation of water vapor,[30,31] and the hydrophobic chemistry was deployed to minimize spectral drift in the real-world sensing scenario, where RH is uncontrolled.

We used a thermal dehydrocoupling chemistry to prepare pSi-Si(C_{18}). As-anodized pSi samples contain a reactive surface chemistry composed of Si−H species that readily undergo dehydrocoupling with a wide range of organic species containing terminal $-SiH_3$ groups.[32] In the present case, the as-etched samples were chemically modified by reaction with octadecylsilane ($H_3Si(CH_2)_{17}CH_3$), which has been shown to impart a highly hydrophobic character.[32] Water contact angle increased from 89° to 128° upon conversion of pSi to pSi-

https://dx.doi.org/10.1021/acssensors.0c01931
ACS Sens. 2021, 6, 418−428

Si(C_{18}) (Figure S2, Supporting Information). Attenuated total reflectance Fourier transform infrared (ATR-FTIR) spectra confirmed the presence of organic signatures assigned to the surface-grafted octadecylsilane species in pSi-Si(C_{18}) (Figure S2, Supporting Information): bands at 1470 and 2850−2930 cm^{-1} are assigned to the scissor and stretching modes of CH_2, respectively. A band at 1080 cm^{-1} is assigned to Si−O stretching; the dehydrocoupling reaction generally produces small quantities of adventitious silicon oxides.[32]

Representative plan-view scanning electron microscope (SEM) images of pSi-Si(C_{18}) (Figure 2a) revealed that the pSi photonic crystals retained their open porous nanostructure after surface functionalization, with a mean pore diameter (ImageJ software, imagej.nih.gov), of 12 ± 3 nm. Furthermore, the cross-sectional SEM images (Figure 2b) revealed the periodic multilayered nanostructure characteristic of the porosity gradient that is generated by the electrochemical preparation and which is responsible for the photonic properties of the material.[29] The porosity and thickness of the octadecyl-modified porous photonic crystals were measured using the spectroscopic liquid infiltration method (SLIM),[29] which indicated a net porosity of ∼30% and an overall thickness of ∼7 μm for the pSi films.

Two colorimetric indicators were chosen based on their known chemical specificity for the HF or HCN analytes of interest in this work. Based on a rhodamine−imidazole complex, RDI has been reported as a selective probe for fluoride that displays a marked change in color due the ability of fluoride to induce a spiro-ring-opening reaction on the rhodamine moiety. RDI was synthesized as previously reported.[33,34] Briefly, the procedure involved reaction of rhodamine 6G with hydrazine to obtain rhodamine hydrazide, and incorporation of the imidazole group to the rhodamine 6G−hydrazide backbone (Figures S3 and S4, Supporting Information). Cobinamide (Cbi), a cobalt-containing Vitamin B-12 analogue, has been used both as an antidote for cyanide poisoning and for analytical applications due to its high affinity for CN^- and its rapid binding kinetics.[35] As-synthesized Cbi contains OH and H_2O ligands coordinated to the cobalt center, and these are sequentially replaced upon encounter with CN^- to generate a 1:2 Cbi:CN^- complex. The binding interactions produce noticeable color changes in Cbi, from orange (absorbance at ∼510 nm) to violet (583 nm). The replacement of OH^- with CN^- results in a strong translabilizing effect, and addition of the second CN^- ligand has been shown to provide a more rapid and more pronounced spectral change in the complex.[36] Thus, in order to enhance the sensing response in this work, the as-synthesized Cbi(OH)(H_2O) complex was titrated with CN^- in a 1:1 molar ratio to generate the monocyano species MCbi, or Cbi(CN)(H_2O), (Figures S5 and S6a, Supporting Information). Calibration curves showing optical absorbance of the MCbi probe at 583 nm as a function of CN^- concentration in water, ethanol, and a 1:1 mixture of water and ethanol are presented in Figure S6b, Supporting Information. The probe showed no detectable solvatochromism. The monocyano complex was diluted with ethanol and loaded into the pSi-Si(C_{18}) matrix to be used as the analyte-selective indicator.

In either case, the RDI or MCbi probes were embedded into the pSi-Si(C_{18}) samples by drop-casting and characterized using ATR-FTIR spectroscopy (Figure S2, Supporting Information). The RDI−pSi-Si(C_{18}) samples showed additional weak bands at 1530 and 1640 cm^{-1} assigned to C−N and amine groups of the RDI probe (Figure S7a, Supporting Information). The MCbi−pSi-Si(C_{18}) samples displayed spectral characteristics of the MCbi probe, with a band at 1670 cm^{-1}, assigned to a C═O stretching mode, as the most distinctive feature (Figure S7b, Supporting Information). The quantity of indicator dye loaded onto the porous samples was optimized to maximize speed and magnitude of response to analyte. The indicator dye of interest was dissolved in solvent and drop-cast onto the pSi-Si(C_{18}) sample, and the quantity of indicator dye delivered to the sample was controlled by control of concentration and drop volume. The mass loading of dye was determined by assuming that all dye in the drop was delivered without loss and that the carrier solvent had completely evaporated. After optimization, the values of mass loading, defined as (mass of dye)/(mass of dye-loaded porous film) were 4.9 ± 0.9% and 2.9 ± 0.3%, for RDI and MCbi samples, respectively. The sensors are referred to in this work as "RDI−pSi-Si(C_{18})" or just "RDI−photonic crystal" (for the HF or DFP sensor) and "MCbi−pSi-Si(C_{18})" or "MCbi−photonic crystal" (for the HCN sensor).

Sensing of HF Using RDI−pSi-Si(C_{18}) Photonic Crystal Sensors. The ability of the RDI−photonic crystal sensors to detect HF in the vapor phase was assessed using a vapor dosing setup fitted with a reflectance spectrometer (see Figure S8, Supporting Information for a schematic and more detailed description of the procedure). Prior to each dosing experiment, the sensors were exposed for 30 min to a flowing gas stream at a fixed value of %RH by premixing a ratio of dry compressed air and air saturated with water vapor, using digital mass flow controllers. The $HF_{(g)}$ analyte was then introduced to the flowing stream by bubbling laboratory air through an aqueous HF solution and diluting it as appropriate using mass flow controllers. The concentration of $HF_{(g)}$ was determined from the dilution ratio and using published partitioning values for $HF_{(g)}$ with $HF_{(aq)}$ at the relevant values of aqueous concentration and temperature, and assuming that the air in the bubbler reached equilibrium with the aqueous solution. Thus, the concentration values for $HF_{(g)}$ given in this work are likely underestimates of the actual values. Based on flow rate and system volume, the time needed to reach steady-state concentration in the sample chamber was ∼8 min.

The response of the RDI−photonic crystal sensor to an HF challenge, measured by optical reflectance spectroscopy, is shown in Figure 3a. As expected, exposure to HF triggered an irreversible increase in optical absorbance at ∼521 nm from the RDI probe molecule due to opening of the spirolactam ring (Figure S9a, Supporting Information), as previously described.[33,34] This increase in absorbance resulted in a decrease in intensity of reflectance from the "Signal" band of the photonic crystal relative to the "Reference" reflectance band. The HF sensing response was quantified with a Response function defined in eq 2:

$$\text{Response} = \frac{R_t}{R_0} = \left(\frac{I_{\text{signal}}}{I_{\text{reference}}}\right)_t \Big/ \left(\frac{I_{\text{signal}}}{I_{\text{reference}}}\right)_0 \quad (2)$$

where R_t is the ratio of intensities of the signal band (I_{signal}) to the reference band ($I_{\text{reference}}$) measured at time t, R_0 is the ratio of intensities of the signal band (I_{signal}) to the reference band ($I_{\text{reference}}$) measured before exposure (time t = 0). The quantity R_0 therefore provided a means to correct for instrumental response at the different wavelengths measured; this is referred to in the figure axes as Normalized $I_{\text{signal}}/I_{\text{reference}}$. A decrease in

https://dx.doi.org/10.1021/acssensors.0c01931
ACS Sens. 2021, 6, 418−428

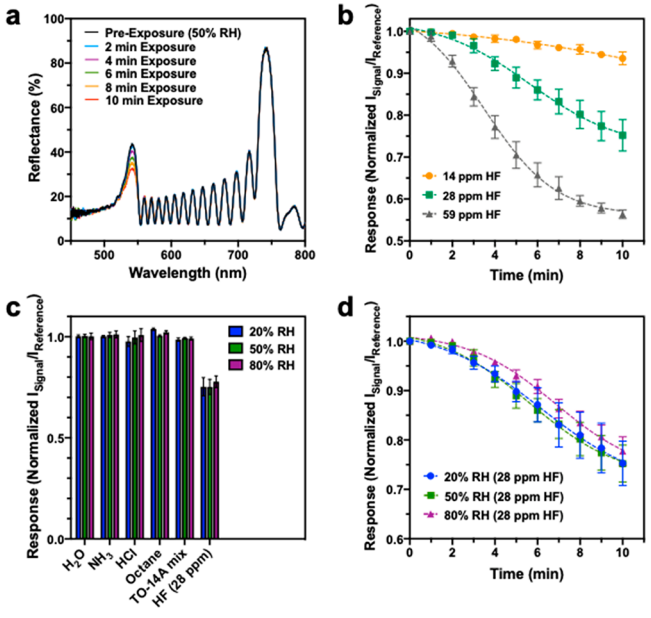

Figure 3. $HF_{(g)}$ sensing performance of RDI−pSi-Si(C_{18}) photonic crystal sensor. (a) Overlaid time series of reflectance spectra obtained from an RDI−pSi-Si(C_{18}) photonic crystal sensor exposed to 28 ppm of $HF_{(g)}$ (50% RH) at the indicated time points. The decrease in the signal peak (~520 nm) indicates detection of HF. (b) Temporal response curves of RDI−pSi-Si(C_{18}) photonic crystal sensors upon exposure to the indicated concentrations of $HF_{(g)}$ (14−59 ppm) at 50% RH. Response metric is defined in eq 2. (c) Selectivity studies of RDI−pSi-Si(C_{18}) photonic crystal sensors challenged with vapors of the indicated potential interferents. Results of experiments performed with carrier gas at 20%, 50%, and 80% RH are shown. Interferent concentrations: NH_3, 100 ppm; HCl, 100 ppm; octane, 600 ppm; and TO-14A mixture of VOCs (0.5 ppm of each component). Bars labeled "H_2O" represent air blanks at the indicated values of RH. Data were acquired 10 min after introduction of the indicated analyte or interferent agents. (d) Temporal response curves for RDI−pSi-Si(C_{18}) photonic crystal sensors upon exposure to 28 ppm of $HF_{(g)}$, measured under varying humidity conditions, as indicated. Error bars shown are the standard deviation from triplicate trials.

the value of this response function corresponds to an increase in absorbance of the indicator dye that correlated with analyte exposure.

Figure 3b presents dose−response curves for the RDI−photonic crystal sensor exposed to $HF_{(g)}$ at concentrations of 14, 28, and 59 ppm, in an air carrier stream maintained at 50% relative humidity (RH). The sensor exhibited a significant decrease in the value of the response function, and the rate of decrease in this value scaled with analyte concentration. For all $HF_{(g)}$ concentrations tested, the responses reached the same (saturation) value after a sufficient period of time had passed (Figure S9b, Supporting Information). This behavior is consistent with the irreversible chemistry of the indicator dye; the saturation level corresponds to a point at which essentially all of the indicator dye available had reacted with HF analyte. Therefore, the response function, and thus the limit of detection (LOD), was a function of both analyte concentration and time of exposure. For example, to reach an LOD (signal exceeding 3 standard deviations relative to the blank) of 28 ppm of $HF_{(g)}$ required 3 min of exposure to the flowing analyte stream, while an LOD of 14 ppm required a 6 min exposure. The time required for the sensor to reliably detect the Immediately Dangerous to Life and Health (IDLH) level of 30 ppm for $HF_{(g)}$ exposure[1] was therefore <3 min. Because of the irreversible kinetics of the spirolactam ring opening reaction of the indicator dye, the behavior of the RDI−photonic crystal system is perhaps more appropriately described as a dosimeter than as a sensor.

We next evaluated the selectivity of the RDI−photonic crystal sensor by comparing the sensor response to $HF_{(g)}$ to the potential interferents ammonia (NH_3), hydrochloric acid (HCl), octane, and a complex air mixture containing 43 different volatile organic compounds defined in method TO-14A by the US Environmental Protection Agency (EPA),[37] referred to in this work as "TO-14A mix." The NH_3, HCl, octane, and TO-14A mix interferents were each diluted into a humidified air stream to achieve 20%, 50%, and 80% RH. The sensors were exposed to a flowing stream of the potential interferents for 10 min, and the responses are presented and compared with a 28 ppm of $HF_{(g)}$ challenge in Figure 3c. The sensors showed no significant response to the NH_3, HCl, and TO-14A mix interferents at all values of %RH tested. The response to octane was also not significant, except for the measurement at RH 20%, where the normalized response was slightly, but significantly (two-way ANOVA, $p < 0.01$) larger compared with the other interferents. The slight increase in the response to octane is attributed to a spectral shift of the stop bands upon infiltration of octane vapor into the mesoporous matrix of the pSi sensor, which led to a slight (<3 nm) red shift upon exposure to 600 ppm of octane (Figure S10, Supporting Information). Because the spectrometer used in these studies was not corrected for its spectral response, a shift in wavelength of the stop band can influence the measured intensity of the band somewhat. These intensity changes were small relative to those seen for the target HF analyte (Figure 3c).

To assess the effect of different RH values on the temporal response of the RDI−photonic crystal sensor, temporal dose−response curves were acquired for a 28 ppm of $HF_{(g)}$ challenge at 20%, 50%, and 80% RH (Figure 3d). The responses of the sensor in 80% RH air were slightly, but consistently suppressed by ~3% relative to the responses measured at 20% and 50% RH. Overall, the sensors displayed a good ability to discriminate HF from the interferents over a wide range of relative humidity values.

Sensing of DFP Using RDI−pSi-Si(C_{18}) Photonic Crystal Sensors. Because it responds to the presence of HF, the RDI−photonic crystal sensor can potentially be used for detection of fluoride-based organophosphonate nerve agents such as sarin, soman, and diisopropyl fluorophosphonate (DFP), as all of these agents are subject to P−F bond hydrolysis, liberating HF as a byproduct.[38] We tested this hypothesis in the case of DFP, a nerve toxin that is considerably less toxic than the organophosphorus nerve agents sarin and soman.[39] The pilot experiments involved generation of DFP vapor using a permeation tube generation system with nitrogen carrier gas at 50 °C. Prior to the dosing of DFP analyte, the sensors were exposed for 30 min to a flowing gas stream at 50% RH by premixing a ratio of nitrogen carrier gas and laboratory air saturated with water vapor. The DFP analyte generated from the permeation tube system (228 ppb) was then introduced into humidified laboratory air to provide the final concentration at 114 ppb DFP vapor at 50% RH. No specific hydrolysis catalyst was used in these experiments, so the generation of the HF analyte needed to activate the RDI−pSi-Si(C_{18}) sensor resulted from the natural,

https://dx.doi.org/10.1021/acssensors.0c01931
ACS Sens. 2021, 6, 418−428

slow rate of hydrolysis of DFP[40] in the mesoporous material,[41] which was not measured here. A ~3% change in the response was observed after 3 h exposure to 114 ppb DFP vapor at 50% RH (Figure S11, Supporting Information). The low level and slow response of the sensor is consistent with the substantially lower concentration of analyte used in these experiments, and the slow kinetics for DFP hydrolysis that can be expected to be present under the test conditions.

Sensing of HCN Using MCbi−pSi-Si(C_{18}) Photonic Crystal Sensors. The MCbi−photonic crystal sensor triggered on the colorimetric change that occurs when the MCbi indicator dye undergoes a binding interaction with cyanide. The response to an HCN vapor challenge is presented in Figure 4. The experiments were performed in a manner

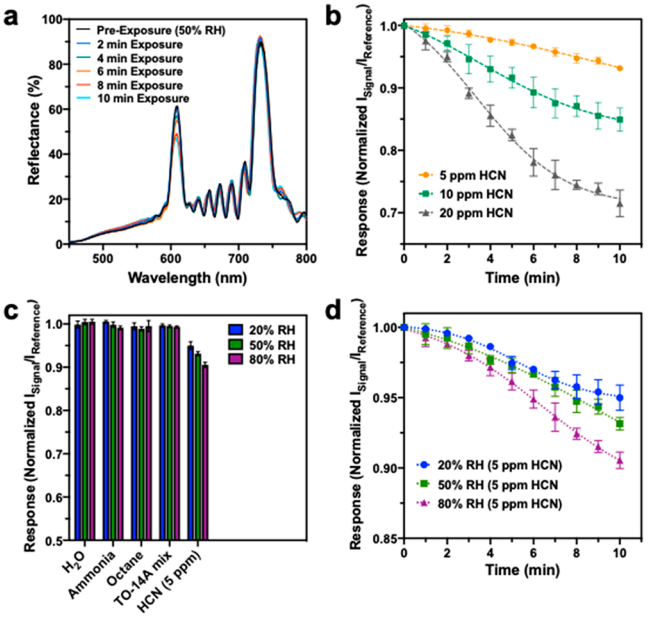

Figure 4. Performance of MCbi−pSi-Si(C_{18}) photonic crystal sensor for HCN detection. (a) Overlaid time series of reflectance spectra obtained from a MCbi−photonic crystal sensor exposed to 20 ppm of $HCN_{(g)}$ (50% RH) at the indicated time points. The decrease in the signal peak (~605 nm) indicates detection of HCN. (b) Temporal response curves of MCbi−photonic crystal sensors upon exposure to the indicated concentrations of HCN vapor under 50% RH. Response metric is defined in eq 2. (c) Selectivity studies of MCbi−photonic crystal sensors challenged with vapors of the indicated potential interferents. Results of experiments performed with carrier gas at 20%, 50%, and 80% RH are shown. Interferent concentrations: NH_3, 100 ppm; octane, 600 ppm; and TO-14A mixture of VOCs (0.5 ppm of each component). Bars labeled "H_2O" represent air blanks at the indicated values of RH. Data were acquired 10 min after introduction of the indicated analyte or interferent agents. (d) Temporal response curves for MCbi−photonic crystal sensors upon exposure to 5 ppm of $HCN_{(g)}$, measured under varying humidity conditions, as indicated. Error bars shown are the standard deviation from triplicate trials.

similar to that involving the RDI−photonic crystal sensors for DFP: the MCbi−photonic crystal sensors were first exposed for 30 min to a humid atmosphere at the desired RH value, and $HCN_{(g)}$ from a calibrated, certified gas cylinder was then introduced into the flow stream (Figure S12, Supporting Information). Reaction of monocyanocobinamide with HCN to form the dicyanocobinamide species generated a broad absorbance band centered at 583 nm (Figure S1, Supporting Information), which overlapped with the 605 nm stop band of the MCbi−photonic crystal sensor. As with the HF sensor, this increase in absorbance resulted in a substantial decrease in the intensity of the "Signal" reflectance peak upon exposure to 20 ppm of $HCN_{(g)}$, with no significant change in the "Reference" reflectance peak of the sensor (Figure 4a). The HCN response was quantified using the Response function defined in eq 2, and the results for the HCN concentration range 5−20 ppm and under 50% RH are presented in Figure 4b. An LOD of 5 ppm of HCN was achieved within 2 min of exposure, whereas the LOD values of 10 and 20 ppm of HCN were achieved within 1 min. Thus, the sensor could detect $HCN_{(g)}$ at the IDLH level (50 ppm)[1] in <1 min.

Although both sensors measured optical absorbance from the indicator dye, the response of the MCbi indicator to $HCN_{(g)}$ differed from the response of the RDI indicator to $HF_{(g)}$ described above because the reaction of MCbi with HCN is reversible. While the equilibrium constant for binding of CN^- to monocyanocobinamide is quite large (~10^8),[36] it was previously demonstrated that the back-reaction is observed when HCN vapor is removed from the gas stream.[42] Consistent with its large binding constant, the rate of loss of CN^- from the dicyano complex of cobinamide was markedly slower than the rate of binding; thus, substantial time was required for the sensor to recover to its original state (Figure S13, Supporting Information).

The selectivity of the MCbi−photonic crystal sensor for $HCN_{(g)}$ relative to the potential interferents ammonia (NH_3), octane, and a mixture of VOCs (TO-14A mix) was quantified at different humidity levels following procedures similar to those described for the $HF_{(g)}$ sensor (i.e., the RDI−photonic crystal). Tests were performed in the absence of the $HCN_{(g)}$ analyte. The NH_3, octane, and TO-14A mix interferents were each diluted into a humidified air stream to achieve 20%, 50%, and 80% RH. The sensors were exposed to a flowing stream of the potential interferents for 10 min, and the responses are presented and compared with a 5 ppm of $HCN_{(g)}$ challenge in Figure 4c. The MCbi−photonic crystal sensor showed no significant response to the NH_3, octane, and TO-14A mix vapor interferents at all values of RH tested. As with the RDI−photonic crystal sensor of Figure 3, the stop bands of the MCbi−photonic crystal sensor displayed slight red shifts upon exposure to 600 ppm of octane vapor (Figure S14, Supporting Information), though in this case it exerted no significant influence on the intensity response function, due to the longer wavelength of the stop band of the "Signal" channel in this sensor type. Similar to the RDI−photonic crystal sensor, the "Signal" stop band of the MCbi−photonic crystal sensor remained within the region of the spectrum where the MCbi dye absorbs for all interferents tested.

The temporal response of the MCbi−photonic crystal sensor to the target HCN analyte was moderately dependent on RH. Temporal response curves acquired for a 5 ppm of $HCN_{(g)}$ challenge at RH values of 20%, 50%, and 80% are presented in Figure 4d. The rate of response of the sensor to $HCN_{(g)}$ increased somewhat with increasing RH, and the dependence of the temporal response on RH was substantial compared to what was observed with the $HF_{(g)}$ sensor (RDI−photonic crystal, Figure 3d). The observed increase in the rate of response to HCN with increasing humidity has been observed previously for the MCbi probe.[34,40] In that prior study, MCbi was dispersed on cellulosic and glass fiber-based paper supports, and it was concluded that the MCbi + HCN reaction chemistry is dependent on the availability of water.

https://dx.doi.org/10.1021/acssensors.0c01931
ACS Sens. 2021, 6, 418−428

That study also found that the sensitivity of the probe to HCN increased with increasing RH. Both of these observations (increase in sensitivity and increase in response rate) are consistent with the present results. The role of water in this reaction is presumably to hydrate and stabilize the dye and to effect deprotonation of HCN into CN^-, in order to form the final cyano-complex with the MCbi probe. The fact that the sensor response is somewhat dependent on humidity imposes a practical limitation on the sensor. However, it should be pointed out that over the entire humidity range studied (20–80% RH), the sensor was able to detect 5 ppm of HCN within 10 min.

Sensing of HF and HCN in a Complex Air Mixture. To simulate real-world environments, the photonic crystal sensors were challenged with their target analytes in the presence of a complex matrix containing multiple VOCs. The experiments described above (Figures 3 and 4) established that the sensors did not respond to the VOCs in the EPA TO-14A calibration mixture (TO-14A mix); however, an additional set of experiments was performed to determine if target analyte detection was obscured in the presence of this more complex sample matrix. The RDI – or MCbi–photonic crystal sensors were exposed to three different conditions in a sequential order: laboratory air (50% RH), air + TO-14A mix at 50% RH, and finally the target analyte (HF or HCN) spiked into air + TO-14A mix at 50% RH (Figure 5). To reduce spectral noise in the intensity measurement (eq 2), each reflectance stop band was fit to a Gaussian function to more accurately determine peak amplitude.

As expected, the ratiometric signal (eq 2) from the RDI– and the MCbi–photonic crystal sensors showed no response to either laboratory air at 50% RH or to 50% RH air containing the TO-14A mix. The sensors then displayed a strong response upon introduction of their target analytes (28 ppm of $HF_{(g)}$ or 10 ppm of $HCN_{(g)}$) into a flowing stream containing the interferents. The response to analyte was slightly slower in the presence of the interferents (Figure 5) relative to what was observed in the absence of the TO-14A mix (Figure 3b and Figure 4b). While it is not surprising that the indicator dyes showed such excellent performance in the complex sample matrix, as they were chosen for this study because of their previously established chemical specificities, these results demonstrated that incorporation of the colorimetric indicators into the mesoporous and hydrophobic environment of the photonic crystal-based sensor did not impair their selectivity.

Remote Sensing Demonstration. The motivation of this study was to improve the fidelity of colorimetric indicator dyes by providing a more distinctive spectral signature that could be discriminated at a distance and in an image field containing substantial spectral or physical "clutter". In the present work, the RDI and MCbi indicator dyes had substantial spectral overlap with each other (Figure 2c and d), such that it would be difficult to distinguish them in a remote image—for example, in a scenario where it was desired to monitor sentinels for multiple threat agents simultaneously. The photonic crystal host then provides an ability to distinguish one sentinel from another, either spectrally or in a hyperspectral image, as the characteristic reflectance band being monitored is artificially narrowed relative to the natural line width of the dye. To evaluate the ability of the approach to be used in a remote sensing scenario, a RDI–photonic crystal sensor was configured in a dosing chamber fitted with an optical window, and the reflectance spectrum was monitored

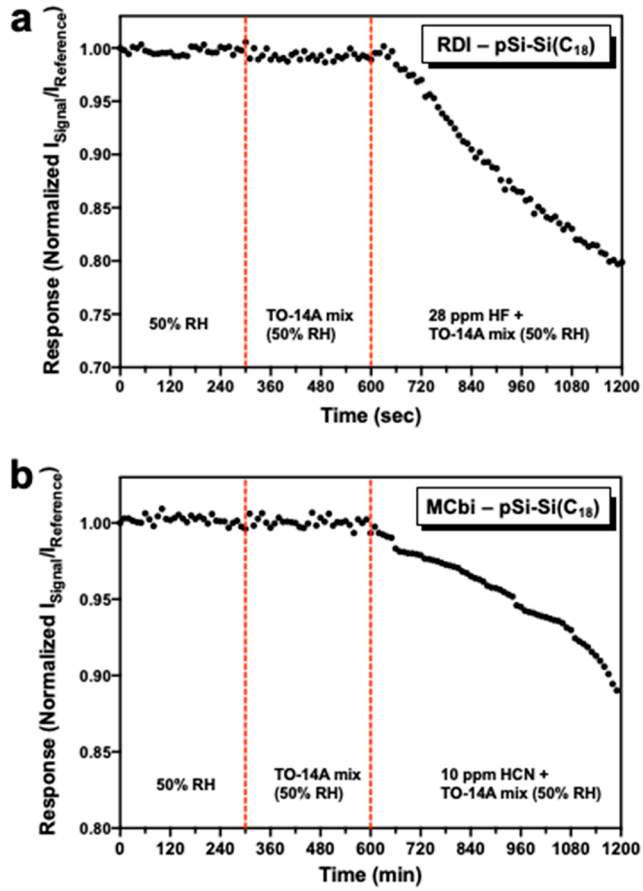

Figure 5. Representative temporal response of (a) RDI–pSi-Si(C_{18}) and (b) MCbi–pSi-Si(C_{18}) photonic crystal sensors to sequential exposure of 50% RH air (time = 0–300 s); TO-14A analyte mixture in 50% RH air (time = 300–600 s); 28 ppm of HF (a) or 10 ppm of HCN (b) in a carrier stream containing TO-14A analyte mixture in 50% RH air (time = 600–1200 s). Each of the 43 VOC components of the TO-14A mixture was present in the air matrix at a nominal concentration of 0.5 ppm. The optical response (as defined in eq 2) were acquired every 10 s.

by a source/detector system fitted to an optical telescope and positioned at a distance 2 m from the sensor (Figure S15a, Supporting Information). The overlaid time-resolved reflectance spectra and temporal response to a 28 ppm of $HF_{(g)}$ challenge (50% RH, in air) were obtained from the RDI–photonic crystal sensor (Figure S15b,c, Supporting Information). Positive detection (95% confidence interval) was confirmed within 3 min of exposure.

In summary, this work showed that a colorimetric dye molecule can be embedded in a mesoporous photonic crystal to provide selective analyte detection that provides a higher degree of fidelity for remote detection by artificially narrowing the spectral bandwidth of the dye. The synthesis of the photonic crystal allowed the creation of specific spectral reflectance signatures that could be engineered to match the dye and to provide a separate reflectance feature that was used as a reference channel in a ratiometric detection scheme. A hydrophobic surface chemistry based on dehydrocoupling of octadecylsilane provided a mesoporous nanostructure that retained sufficient porosity to host the indicator dye and to allow ingress of the gas-phase analytes, while suppressing zero-point drift due to fluctuations in relative humidity, which was established over the range 20–80% RH. The two types of

https://dx.doi.org/10.1021/acssensors.0c01931
ACS Sens. 2021, 6, 418–428

sensors, RDI−pSi-Si(C_{18}) photonic crystal for HF and MCbi−pSi-Si(C_{18}) photonic crystal for HCN, were able to detect their analytes at levels below the NIOSH IDLH. Due to its similar indicator chemistry, which triggered on the presence of HF, the RDI−photonic crystal was also able to detect the fluorophosphonate nerve agent DFP at a level of 114 ppb. For irreversible indicator chemistries, such as the RDI dye used in this work to detect HF, the sensor displayed behavior similar to a dosimeter, where the rate of change in response scaled with concentration, but reached a point of saturation at exposure times sufficiently long to allow reaction of the dye with the analyte to reach completion. Both types of sensors were stable in ambient laboratory air and showed excellent selectivity for their target analyte relative to interferents NH_3, HCl, octane, or a complex mixture of VOCs (EPA TO-14A).

EXPERIMENTAL SECTION

Materials. Single-crystal highly doped p-type (B-doped) silicon wafers of resistivity 0.8−1 mΩ-cm, polished on the (100) face, were purchased from Siltronix Corp. All reagents were used as received. Octadecylsilane ($H_3Si(CH_2)_{17}CH_3$) was purchased from Gelest, Inc. Diisopropyl fluorophosphonate was purchased from Sigma-Aldrich, catalogue #D0879, while the permeation tube was purchased from Kin-Tek Analytical, catalogue #143409, calibrated at a concentration of 0.228 ppm DFP (at a flow rate of 50 sccm). Premixed hydrogen cyanide gas cylinders (10 and 20 ppm; balance gas nitrogen) were purchased from Gasco Inc. EPA TO-14A Calibration mix was purchased from Restek through Linde Spectra Environmental Gases, catalogue #34432 and contained 1 ppm of each component. All other chemical reagents were purchased from Sigma-Aldrich.

Instrumentation. Attenuated total reflectance Fourier transform infrared (ATR-FTIR) spectra were recorded on a Thermo Scientific Nicolet 6700 FTIR instrument fitted with a Smart iTR diamond ATR fixture. Scanning electron microscope (SEM) images were obtained with a Zeiss Sigma 500 in secondary electron imaging mode. Contact angles were measured using a Rame-Hart DROPimage CA v2.5 instrument. Reflected light spectra were obtained in the visible-NIR spectral range with an Ocean Optics USB-4000 CCD spectrometer and a tungsten-halogen illumination source (Ocean Optics LS-1) connected with a Y-branch 600-μm-diameter, bifurcated multimode optical fiber. The common end of the bifurcated fiber was focused with an objective lens to a ∼1 mm^2 spot and positioned with the optic axis normal to the sample surface. UV−vis absorbance spectra were obtained using a Molecular Devices SpectraMax 340PC384 Microplate Spectrophotometer with a 1 cm path length cuvette and 96-well microplate with normalized absorbance values to an equivalent 1 cm path length cuvette. 1H NMR analysis was performed on a Varian spectrometer running at 500 MHz, or a 300 MHz Bruker AVA. Mass spectrometry analysis was performed by the University of California San Diego Chemistry and Biochemistry Mass Spectrometry Facility (MMSF). The ESI-MS spectrum of Cbi was obtained using an Otribtrap Exactive mass spectrometer (Thermo Fisher, San Jose, CA, USA) with an ESI source at capillary temperature of 275 °C and spray voltage of 3.5 kV in positive ion mode. The spectra were acquired for m/z = 75−1500 using a maximum injection time of 50 ms and a resolution of 100,000. Prior to this, all the Cbi samples were diluted 50-fold with methanol containing 0.25% by mass formic acid. Diluted samples were directly infused into the mass spectrometer at a rate of 5 μL/min.

Preparation of pSi Photonic Crystals. The single-crystal Si wafers were diced into square chips of approximately 2 × 2 cm^2 and mounted in a Teflon etching cell described elsewhere. The O-ring seal of the cell exposed 1.2 cm^2 of the Si surface to electrolyte. The chip was contacted on the backside with aluminum foil, and the counter-electrode consisted of a platinum coil. The chip was anodized in an electrolyte consisting of 3:1 (v:v) 48% aqueous hydrofluoric acid:ethanol (CAUTION: HF is highly toxic and can cause severe burns on contact with the skin or eyes). Prior to the preparation of the porous layers, the samples were cleaned using a "sacrificial etch" which consisted of etching a thin pSi layer into the chip (400 mA cm^{-2} applied for 50 s) in the above electrolyte, removing the electrolyte, rinsing the cell with ethanol, and then dissolving this layer in strong base (2 M aqueous KOH). The cell was then rinsed with water and ethanol, fresh aqueous HF:ethanol electrolyte was added, and the cleaned sample was anodized to prepare the photonic crystal. The anodization waveform for the photonic crystal was generated using LabView (National Instruments, Inc.), and the electric current was driven by a Keithley 2651A Sourcemeter power supply interfaced to the LabView program. The time-dependent current density waveforms, $J(t)$, used in this work were created following the relationship of eq 1, with J_{min} = 4.167 mA/cm^2, J_{max} = 60.0 mA/cm^2. For the HF and DFP sensors (RDI−pSi-Si(C_{18}) photonic crystal), values of T_1 = 6.6 s and T_2 = 9.8 s were used. For the HCN sensors (MCbi−pSi-Si(C_{18}) photonic crystal), values of T_1 = 8 s and T_2 = 9.8 s were used. The etching waveform was applied for 300 s. The as-etched samples were then chemically modified by subjecting them to a dehydrocoupling reaction with *n*-octadecylsilane: 500 μL of *n*-octadecylsilane, $H_3Si(CH_2)_{17}CH_3$, was introduced via microliter syringe to the pSi photonic crystal substrate in a 20 mL vial. The vial was sealed and immersed in a silicone oil bath at 80 °C for 16 h. The samples were then cooled, removed, and rinsed 3× with *n*-hexane and then 3× with ethanol.

Synthesis of Rhodamine 6G Imidazole (RDI). Rhodamine 6G hydrazide was synthesized following the procedure previously described.[32,33] Rhodamine 6G (2.40 g, 5 mmol) was dissolved in ethanol (60 mL). Hydrazine monohydride (8 mL, 160 mmol) was added, and the reaction was maintained at reflux for 2 h, then allowed to stir overnight at room temperature. The white precipitate was filtered and washed with water and ethanol to yield the product, rhodamine 6G hydrazide (1.68 g, 79%). The product was used for the next step without further purification. To prepare rhodamine 6G imidazole (RDI), rhodamine 6G hydrazide (0.5 g, 1.17 mmol) was dissolved in methanol (10 mL). 2-Formylimidazole was then added, and the reaction was maintained at reflux overnight. The precipitate was filtered, washed with ethanol, and dried *in vacuo* (yield: 0.20 g, 35%).

Synthesis of Monocyanocobinamide (MCbi). Pure aquohydroxocobinamide [$OH(H_2O)$Cbi], Co(III) was synthesized by base hydrolysis of hydroxocobalamin as described previously.[35] A stock solution of monocyanocobinamide ($CN(H_2O)$Cbi) was then prepared by reacting a 1:1 equimolar amount of aquohydroxocobinamide with KCN dissolved in deionized water in 1 M aqueous NaOH for 6 h under mild agitation at room temperature, resulting in a dark red solution. Using a benchtop optical absorbance spectrometer (Molecular Devices Spectramax 340Pc384 Microplate Spectrophotometer), the distinct absorbance band at 475−520 nm confirmed the synthesis of monocyanocobinamide.

Loading of Colorimetric Indicators. For the RDI−photonic crystal sensors (HF or DFP analytes), the rhodamine−imidazole (RDI) complex was dissolved in a 1:1 (v:v) dichloromethane:acetonitrile mixture at a concentration of 1 mg/mL. A 100 μL aliquot of RDI was then drop-cast onto the pSi-Si(C_{18}) photonic crystal substrate and allowed to dry at room temperature. For HCN sensing, a monocyanocobinamide (MCbi) stock solution was diluted in ethanol until the concentration of the solution was 500 μM. A 100 μL aliquot of MCbi solution was subsequently drop-cast onto pSi-Si(C_{18}) photonic crystal substrates and allowed to dry in air at room temperature for ∼5 h or until the ethanol solvent appeared fully evaporated. The majority of the finished sensors were stored in ambient laboratory air for 1−3 days prior to testing; no apparent degradation in the analyte responses due to such storage was observed.

Vapor Dosing Experiments. Analyte vapor challenges were prepared by dilution of analyte vapor streams of fixed concentration with dry or humidified compressed air, laboratory air, or nitrogen gas using digital mass flow controllers to obtain the desired concentration. For hydrogen fluoride, hydrogen chloride, and ammonia, aqueous solutions of these analytes were prepared at a given concentration,

https://dx.doi.org/10.1021/acssensors.0c01931
ACS Sens. 2021, 6, 418−428

and the vapors were generated by bubbling the laboratory air through them. Details are provided in Figure S8, Supporting Information. Octane vapor was generated by bubbling the laboratory air though neat octane. For hydrogen cyanide and EPA TO-14A mix, the gas produced directly from the certified gas cylinder was mixed with humidified laboratory air to the desired concentration. The concentrations of analytes were calculated based on their partial pressures at 25 °C over the aqueous solution (for HF, HCl, and NH_3) or the neat liquid (for octane);[43−45] the partial pressures of analyte vapors were then converted to concentration using eq 3:[46]

$$\text{Vapor concentration(ppm)} = \frac{P_{\text{analyte}}}{760\ \text{mmHg}} \times 10^6 \times \frac{F_{\text{analyte}}}{F_{\text{analyte}} + F_{\text{dilutionair}}} \quad (3)$$

where P_{analyte} is the partial pressure of the analyte vapor, in Torr, F_{analyte} is the flow rate of the analyte vapor stream in sccm, and $F_{\text{dilution air}}$ is the flow rate of the dilution air stream in sccm.

For the DFP experiments, the vapor was generated from a certified permeation tube (Kin-Tek Analytical, catalogue #143409) that was heated to 50 °C in a Metronics Inc. VICI Dynacalibrator Model 190 permeation oven, producing 228 ppb of DFP vapor in a nitrogen carrier gas. This was then mixed 1:1 (v:v) with humid laboratory air to achieve the desired humidity (50% RH) and analyte concentration (114 ppb). The RH values reported were verified with a probe hygrometer. The DFP sensing experiment was conducted with a net flow rate of 100 sccm; all the other sensing experiments were conducted with a net flow rate of 300 sccm.

Reflectance spectra from the sensors were collected with a CCD spectrometer (Ocean Optics USB-4000) coupled to one branch of a bifurcated fiber optic cable. Light from a tungsten filament source was fed into the other branch of the fiber. The two branches were combined to a single fiber, and a focusing or a collimating lens was fitted to the distal end of this combined fiber and mounted 20 cm above or 2 m in front of the samples in the test chamber.

■ ASSOCIATED CONTENT

Supporting Information

The Supporting Information is available free of charge at https://pubs.acs.org/doi/10.1021/acssensors.0c01931.

UV−vis absorbance spectra and calibration curves for RDI and MCbi indicator dyes as a function of analyte concentration; Water contact angle images, FTIR spectra of pSi photonic crystal sensors; ^{1}H NMR and Mass spectra of RDI and Cbi dyes; Images of cobinamide solutions at various stages of titration with HCN; ATR-FTIR spectra of RDI and Cbi dry powder samples; schematics of vapor dosing setup for HF-sensing experiment; schematic mechanism of RDI reaction with HF and temporal response curves for RDI−pSi-Si(C_{18}) photonic crystal sensors exposed to $HF_{(g)}$; temporal response curve of RDI−pSi-Si(C_{18}) photonic crystal sensor exposed to DFP vapor; schematics of vapor dosing setup for HCN^- sensing experiment; experimental setup for remote sensing of HF vapor (PDF)

■ AUTHOR INFORMATION

Corresponding Author

Michael J. Sailor − *Materials Science and Engineering Program and Department of Chemistry and Biochemistry, University of California, San Diego, La Jolla, California 92093, United States;* orcid.org/0000-0002-4809-9826; Email: msailor@ucsd.edu

Authors

Yi-Sheng Lu − *Materials Science and Engineering Program, University of California, San Diego, La Jolla, California 92093, United States*

Sanahan Vijayakumar − *Materials Science and Engineering Program, University of California, San Diego, La Jolla, California 92093, United States*

Arnaud Chaix − *Department of Chemistry and Biochemistry, University of California, San Diego, La Jolla, California 92093, United States*

Brian R. Pimentel − *Department of Chemistry and Biochemistry, University of California, San Diego, La Jolla, California 92093, United States*

Kyle C. Bentz − *Department of Chemistry and Biochemistry, University of California, San Diego, La Jolla, California 92093, United States*

Sheng Li − *Department of Medicine, University of California, San Diego, La Jolla, California 92093, United States*

Adriano Chan − *Department of Medicine, University of California, San Diego, La Jolla, California 92093, United States*

Charlotte Wahl − *Leidos, San Diego, California 92121, United States*

James S. Ha − *Leidos, San Diego, California 92121, United States*

Deborah E. Hunka − *Leidos, San Diego, California 92121, United States*

Gerry R. Boss − *Department of Medicine, University of California, San Diego, La Jolla, California 92093, United States*

Seth M. Cohen − *Materials Science and Engineering Program and Department of Chemistry and Biochemistry, University of California, San Diego, La Jolla, California 92093, United States;* orcid.org/0000-0002-5233-2280

Complete contact information is available at: https://pubs.acs.org/10.1021/acssensors.0c01931

Notes

The authors declare the following competing financial interest(s): M.J.S. is a scientific founder of Spinnaker Biosciences, Inc., a member of the Board of Directors, and has an equity interest in the company; he is a scientific founder of Impilo Therapeutics, Inc., a member of the Board of Directors, and has an equity interest in the company. M.J.S. is a consultant, shareholder, or scientific advisor for Bejing ITEC Technologies, Cend Therapeutics, Illumina, Matrix Technologies, NanoVision Bio, Pacific Integrated Energy, TruTags, and Well-Healthcare Technologies. M.J.S. is a Guest Professor at Zhejiang University, China. Although one or more of the grants that supported this research has been identified for conflict of interest management based on the overall scope of the project and its potential benefit to the above companies, the research findings included in this particular publication may not necessarily relate to their interests. The terms of this arrangement have been reviewed and approved by the University of California, San Diego in accordance with its conflict of interest policies.

■ ACKNOWLEDGMENTS

The research is based upon work supported by the office of the Director of National Intelligence (ODNI), Intelligence Advanced Research Projects Activity (IARPA), under contract

number 2018-18071700005, by the UC San Diego Materials Research Science and Engineering Center (UCSD MRSEC) supported by the National Science Foundation (Grant DMR-2011924), and by the San Diego Nanotechnology Infrastructure (SDNI) of UCSD, a member of the National Nanotechnology Coordinated Infrastructure, which is supported by the National Science Foundation (Grant ECCS-1542148). The views and conclusions contained herein are those of the authors and should not be interpreted as necessarily representing the official policies or endorsements, either expressed or implied, of the ODNI, IARPA, or the U.S. Government. The U.S. Government is authorized to reproduce and distribute reprints for Governmental purposes notwithstanding any copyright annotation thereon. Specifically, the contract funded Y−S. L., S.V., A.C., B.R.P., and K.C.B. S.V. also acknowledges support from the UC San Diego Jacobs School of Engineering Cal RA. The authors thank Jinkyue Ree for discussions regarding the development of the vapor dosing system. K.C.B. acknowledges support from the Research Corporation for Scientific Advancement (RCSA) through the Cottrell Fellowship Initiative, which is partially funded by a National Science Foundation award to the RCSA (CHE-2039044).

REFERENCES

(1) *NIOSH Pocket Guide to Chemical Hazards*; DHHS (NIOSH) Publication #2005−149, National Institute for Occupational Safety and Health of the United States: Cincinnati, OH, 2007.

(2) Kim, K.; Tsay, O. G.; Atwood, D. A.; Churchill, D. G. Destruction and Detection of Chemical Warfare Agents. *Chem. Rev.* **2011**, *111*, 5345−5403.

(3) Alcaraz, A. Gas Chromatography/Mass Spectrometry in Analysis of Chemicals Relevant to the Chemical Weapons Convention Update based on the original article by Eric R.J. Wils. In *Encyclopedia of Analytical Chemistry*, Meyers, R. A.; Meyers, R. A., Eds.; John Wiley & Sons, Ltd.: New Jersey, 2012. DOI: 10.1002/9780470027318.a0405.pub2.

(4) Mäkinen, M. A.; Anttalainen, O. A.; Sillanpää, M. E. T. Ion Mobility Spectrometry and Its Applications in Detection of Chemical Warfare Agents. *Anal. Chem.* **2010**, *82*, 9594−9600.

(5) Mosier-Boss, P. A. Review of SERS Substrates for Chemical Sensing. *Nanomaterials* **2017**, *7*, 142.

(6) Kondo, T.; Hashimoto, R.; Ohrui, Y.; Sekioka, R.; Nogami, T.; Muta, F.; Seto, Y. Analysis of chemical warfare agents by portable Raman spectrometer with both 785nm and 1064nm excitation. *Forensic Sci. Int.* **2018**, *291*, 23−38.

(7) Hodgkinson, J.; Tatam, R. P. Optical gas sensing: a review. *Meas. Sci. Technol.* **2013**, *24*, 012004.

(8) U.S. Department of Homeland Security, System Assessment and Validation for Emergency Responders (SAVER), *Portable Infrared Spectroscopy Chemical Detectors Assessment Report*; Richland, WA, 2016.

(9) Grate, J. W. Acoustic Wave Microsensor Arrays for Vapor Sensing. *Chem. Rev.* **2000**, *100*, 2627−2648.

(10) Janata, J.; Josowicz, M. Conducting polymers in electronic chemical sensors. *Nat. Mater.* **2003**, *2*, 19−24.

(11) Wetchakun, K.; Samerjai, T.; Tamaekong, N.; Liewhiran, C.; Siriwong, C.; Kruefu, V.; Wisitsoraat, A.; Tuantranont, A.; Phanichphant, S. Semiconducting metal oxides as sensors for environmentally hazardous gases. *Sens. Actuators, B* **2011**, *160*, 580−591.

(12) Zhou, X.; Lee, S.; Xu, Z.; Yoon, J. Recent Progress on the Development of Chemosensors for Gases. *Chem. Rev.* **2015**, *115*, 7944−8000.

(13) Liu, Y.; Hu, Y.; Lee, S.; Lee, D.; Yoon, J. Fluorescent and Colorimetric Chemosensors for Anions, Metal Ions, Reactive Oxygen Species, Biothiols, and Gases. *Bull. Korean Chem. Soc.* **2016**, *37*, 1661−1678.

(14) Chen, L.; Wu, D.; Yoon, J. Recent Advances in the Development of Chromophore-Based Chemosensors for Nerve Agents and Phosgene. *ACS Sens.* **2018**, *3*, 27−43.

(15) Lim, S. H.; Feng, L.; Kemling, J. W.; Musto, C. J.; Suslick, K. S. An optoelectronic nose for the detection of toxic gases. *Nat. Chem.* **2009**, *1*, 562−567.

(16) Davidson, C. E.; Dixon, M. M.; Williams, B. R.; Kilper, G. K.; Lim, S. H.; Martino, R. A.; Rhodes, P.; Hulet, M. S.; Miles, R. W.; Samuels, A. C.; Emanuel, P. A.; Miklos, A. E. Detection of Chemical Warfare Agents by Colorimetric Sensor Arrays. *ACS Sens.* **2020**, *5*, 1102−1109.

(17) Liu, X.; Cheng, S.; Liu, H.; Hu, S.; Zhang, D.; Ning, H. A survey on gas sensing technology. *Sensors* **2012**, *12*, 9635−9665.

(18) Hou, C.; Li, J.; Huo, D.; Luo, X.; Dong, J.; Yang, M.; Shi, X. A portable embedded toxic gas detection device based on a cross-responsive sensor array. *Sens. Actuators, B* **2012**, *161*, 244−250.

(19) Devadhasan, J. P.; Kim, D.; Lee, D. Y.; Kim, S. Smartphone coupled handheld array reader for real-time toxic gas detection. *Anal. Chim. Acta* **2017**, *984*, 168−176.

(20) Askim, J. R.; Suslick, K. S. Hand-Held Reader for Colorimetric Sensor Arrays. *Anal. Chem.* **2015**, *87*, 7810−7816.

(21) Kassal, P.; Horak, E.; Sigurnjak, M.; Steinberg, M. D.; Steinberg, I. M. Wireless and mobile optical chemical sensors and biosensors. *Rev. Anal. Chem.* **2018**, *37*, 20170024.

(22) Luka, G. S.; Nowak, E.; Kawchuk, J.; Hoorfar, M.; Najjaran, H. Portable device for the detection of colorimetric assays. *R. Soc. Open Sci.* **2017**, *4*, 171025−171025.

(23) Switkes, M.; Ervin, B. L.; Kingsborough, R. P.; Rothschild, M.; Sworin, M. Retroreflectors for remote readout of colorimetric sensors. *Sens. Actuators, B* **2011**, *160*, 1244−1249.

(24) King, B. H.; Gramada, A.; Link, J. R.; Sailor, M. J. Internally Referenced Ammonia Sensor Based on an Electrochemically Prepared Porous SiO2 Photonic Crystal. *Adv. Mater.* **2007**, *19*, 4044−4048.

(25) Garcia Sega, A.; King, B. H.; Lee, J. Y.; Sailor, M. J.; Miskelly, G. M. Thermally Modulated Porous Silica Multispectral Filters and Their Application in Remote Imaging. *ACS Nano* **2013**, *7*, 7785−7794.

(26) Ruminski, A. M.; Barillaro, G.; Chaffin, C.; Sailor, M. J. Internally Referenced Remote Sensors for HF and Cl2 Using Reactive Porous Silicon Photonic Crystals. *Adv. Funct. Mater.* **2011**, *21*, 1511−1525.

(27) Leacock-Johnson, A.; Garcia Sega, A.; Sharief, A.; Sailor, M. J.; Miskelly, G. M. Real-time 1D hyperspectral imaging of porous silicon-based photonic crystals with one-dimensional chemical composition gradients undergoing pore-filling-induced spectral shifts. *Sens. Actuators, A* **2013**, *203*, 154−159.

(28) Weiss, S. M.; Molinari, M.; Fauchet, P. M. Temperature stability for silicon-based photonic band-gap structures. *Appl. Phys. Lett.* **2003**, *83*, 1980−1982.

(29) Sailor, M. J. *Porous Silicon in Practice: Preparation, Characterization, and Applications*; Wiley-VCH: Weinheim, Germany, 2012.

(30) Ruminski, A. M.; King, B. H.; Salonen, J.; Snyder, J. L.; Sailor, M. J. Porous Silicon-Based Optical Microsensors for Volatile Organic Analytes: Effect of Surface Chemistry on Stability and Specificity. *Adv. Funct. Mater.* **2010**, *20*, 2874−2883.

(31) Ruminski, A. M.; Moore, M. M.; Sailor, M. J. Humidity-Compensating Sensor for Volatile Organic Compounds Using Stacked Porous Silicon Photonic Crystals. *Adv. Funct. Mater.* **2008**, *18*, 3418−3426.

(32) Kim, D.; Joo, J.; Pan, Y.; Boarino, A.; Jun, Y. W.; Ahn, K. H.; Arkles, B.; Sailor, M. J. Thermally Induced Silane Dehydrocoupling on Silicon Nanostructures. *Angew. Chem., Int. Ed.* **2016**, *55*, 6423−6427.

(33) Zhang, Z.; Zheng, Y.; Hang, W.; Yan, X.; Zhao, Y. Sensitive and selective off-on rhodamine hydrazide fluorescent chemosensor for hypochlorous acid detection and bioimaging. *Talanta* **2011**, *85*, 779−786.

(34) Sivaraman, G.; Chellappa, D. Rhodamine based sensor for naked-eye detection and live cell imaging of fluoride ions. *J. Mater. Chem. B* **2013**, *1*, 5768−5772.
(35) Greenawald, L. A.; Snyder, J. L.; Fry, N. L.; Sailor, M. J.; Boss, G. R.; Finklea, H. O.; Bell, S. Development of a cobinamide-based end-of-service-life indicator for detection of hydrogen cyanide gas. *Sens. Actuators, B* **2015**, *221*, 379−385.
(36) Ma, J.; Dasgupta, P. K.; Zelder, F. H.; Boss, G. R. Cobinamide chemistries for photometric cyanide determination. A merging zone liquid core waveguide cyanide analyzer using cyanoaquacobinamide. *Anal. Chim. Acta* **2012**, *736*, 78−84.
(37) Manning, J. A.; Burckle, J. O.; Hedges, S.; McElro, F. F. Compendium Method TO-14A. *Compendium of Methods for the Determination of Toxic Organic Compounds in Ambient Air* 2nd ed.; Environmental Protection Agency: 1999.
(38) Hammond, P.; Forster, J. A polymeric amine-copper(II) complex as catalyst for the hydrolysis of 1,2,2-trimethylpropyl methylphosphonofluoridate (soman) and bis (1-methylethyl) phosphorofluoridate (DFP). *J. Appl. Polym. Sci.* **1991**, *43*, 1925−1931.
(39) Misik, J.; Pavlikova, R.; Cabal, J.; Kuca, K. Acute toxicity of some nerve agents and pesticides in rats. *Drug Chem. Toxicol.* **2015**, *38*, 32−36.
(40) Kilpatrick, M.; Kilpatrick, M. L. The Hydrolysis of Diisopropyl Fluophosphate. *J. Phys. Colloid Chem.* **1949**, *53*, 1371−1384.
(41) Baldwin, D. S.; Beattie, J. K.; Coleman, L. M.; Jones, D. R. Phosphate Ester Hydrolysis Facilitated by Mineral Phases. *Environ. Sci. Technol.* **1995**, *29*, 1706−1709.
(42) Greenawald, L. A.; Boss, G. R.; Snyder, J. L.; Reeder, A.; Bell, S. Development of an Inexpensive RGB Color Sensor for the Detection of Hydrogen Cyanide Gas. *ACS Sens.* **2017**, *2*, 1458−1466.
(43) Brosheer, J.; Lenfesty, F.; Elmore, K. Vapor Pressure of Hydrofluoric Acid Solutions. *Ind. Eng. Chem.* **1947**, *39*, 423−427.
(44) Fritz, J. J.; Fuget, C. R. Vapor Pressure of Aqueous Hydrogen Chloride Solutions, O° to 50° C. *Chem. Eng. Data Ser.* **1956**, *1*, 10−12.
(45) Clegg, S.; Brimblecombe, P. Solubility of ammonia in pure aqueous and multicomponent solutions. *J. Phys. Chem.* **1989**, *93*, 7237−7248.
(46) Woodfin, W. J. *Gas and vapor generating systems for laboratories*; U.S. Dept. of Health, Education and Welfare, Public Health Service, Center for Disease Control, National Institute for Occupational Safety and Health, Division of Physical Sciences and Engineering: Cincinnati, OH, 1984.

https://dx.doi.org/10.1021/acssensors.0c01931
ACS Sens. 2021, 6, 418−428